IEEE Access
Multidisciplinary | Rapid Review | Open Access Journal

Received May 7, 2021, accepted May 27, 2021, date of publication June 2, 2021, date of current version June 9, 2021.

Digital Object Identifier 10.1109/ACCESS.2021.3085298

A Double-Terminal Traveling-Wave-Based Method Using Novel Noncontact Sensors for Fault Location in Transmission Cable Lines

MING ZHANG[1], KUN ZHAO[2], (Student Member, IEEE), YUAN YAN[2], YUXIN LU[2], SAIKE YANG[2], LI WANG[2], AND HONGJIE LI[2]

[1]Foshan Electric Power Station of Guangdong Power Grid Company Ltd., Foshan 528000, China
[2]School of Electrical Engineering, Xi'an Jiaotong University, Xi'an 710049, China

Corresponding author: Hongjie Li (hjli@mail.xjtu.edu.cn)

This work was supported by Guangdong Power Grid Company Ltd., under Project 030600KK52170101.

ABSTRACT The burgeoning demand for enhanced power-system safety means that there is increased attention on technologies for the detection and location of cable faults. The double-terminal fault location method, which senses a fault current using a current transformer (CT), is the most effective and widely applied method in industrial practice. However, CT sensors may suffer from magnetic saturation when exposed to a high fault current, resulting in significant location errors, and their sensitivity cannot be adjusted. To address this problem, this paper describes an improved method for the acquisition of fault signal and the identification of fault-wave arrival time in power cables. First, a novel noncontact sensor (NCS) is developed for the detection of electric fields, and its sensitivity-adjustment curves are obtained by theoretical calculation and simulation. Then, based on feedback variational mode decomposition (FVMD) and the Wigner–Ville distribution (WVD), an improved method (the FVMD + WVD method) for the identification of fault-wave arrival time is devised, and its efficacy and accuracy are verified by simulations in Power Systems Computer-Aided Design/Electromagnetic Transients including DC (PSCAD/EMTDC) software. Finally, the fault-wave arrival-time detection performance of the NCS is examined in a series of on-site DC and AC experiments based on damped AC technology. The results show that the NCS exhibits feasible and effective performance, and that its response can be appropriately tuned based on its sensitivity-adjustment curves. The FVMD + WVD method is more accurate than several other current methods, as its error is only 0.48%, and thus this method enables the practical location of cable faults. In sum, these findings demonstrate that the NCS and the FVMD + WVD method comprise an improved system for the detection and location of cable faults, which will enhance cable safety in power systems.

INDEX TERMS Fault detection and location, double-terminal, electric field sensors, feedback variational mode decomposition, Wigner-Ville distribution.

I. INTRODUCTION

The development of the global economy is resulting in increased electricity consumption, which is leading to a burgeoning demand for highly reliable power cables. Faulty power cables have profound negative effects on societal functioning, and thus power outage time must be minimized. In recent years, electrical-energy administrators in China have addressed this need by stipulating that fault-monitoring auxiliary modules should be installed on power cables. In addition, effective methods must be developed to detect and locate power cable faults. Such methods are typically classified as offline or online methods [1]–[3]. Common offline methods are tracer methods, time-domain reflectometer methods, and the bridge method [4], [5], and although these are accurate and reliable, they are also labor- and time-intensive. Online methods are categorized as impedance-based methods or traveling-wave methods [6]–[8]. It is well-established that impedance-based methods are effective [9]–[13] but they are easily affected

The associate editor coordinating the review of this manuscript and approving it for publication was Guangya Yang.

by the end source. Traveling methods are categorized as single- or double-terminal fault-location methods [14]–[16], and the development of inexpensive communications and accurate satellite-time services has led to double-terminal fault-location methods becoming common. Machine learning methods, such as convolution neural networks, are also used in fault location, and are greatly effective in some situations [17]. However, although the theory of many fault location methods has been researched, few have been tested in practice.

The double-terminal method is an effective means of detecting cable faults and is thus widely used. It is based on time synchronization, signal acquisition, and fault-wave arrival-time identification. The development of the global positioning system (GPS) and the BeiDou navigation system (BDS) has largely solved the problem of time synchronization, but signal acquisition and fault-wave arrival-time identification methods remain areas of intense study. Sensors play a key role in signal acquisition, and high-frequency current transformer (HFCT) sensors are the most widely used due to their isolatability [18]–[21]. However, the functional limitations of ferromagnetic cores and coils mean that the sensitivity of HFCT sensors cannot be adjusted, and the cores are easily saturated [22]. In addition, to enable a sensor to detect signals, an extra ground wire from the equipment must cross an HFCT, affecting the safety of the equipment. There is therefore a need for a reliable sensor with adjustable sensitivity and a safer operational profile than HFCT sensors.

Methods for the analysis of arrival time are classified as time-domain methods or frequency-domain methods [23], [24]. Time-domain methods include those based on peak detection, an energy criterion, the Akaike information criterion, or Gabor's signal centroid, and are simple but prone to noise and pulse effects. Frequency-domain methods include those based on the sliding discrete Fourier transform (SDFT), discrete wavelet transforms (DWTs), and empirical mode decomposition (EMD). SDFT methods cannot detect arrival time with adequate time resolution, which leads to increased errors in fault location. DWT methods use various mother wavelets to detect arrival time but are only accurate if the shape of a selected mother wavelet is similar to that of the fault wave. Thus, other frequency-domain methods have been studied, such as EMD methods. However, these are based on the Hilbert transform, which has no strict mathematical proof, and EMD have frequency aliasing phenomenon so more error are introduced in fault location [25], [26].

To solve the above problems, a novel noncontact sensor (NCS) is developed to detect fault signals in an electric field. Then, a method that is a combination of feedback variational mode decomposition (FVMD) and the Wigner-Ville distribution (WVD), and thus capable of considering the time and frequency domains, is developed and used to identify the arrival times of the first fault waves. This method is simulated and estimated in Power Systems Computer-Aided Design/Electromagnetic Transients including DC (PSCAD/EMTDC) software. Finally, the reliability and accuracy of the NCS and the developed method are tested using a damped AC (DAC) system in an out-of-service cable line.

The remainder of this paper is organized as follows. In Section II, basic principles (such as monitoring systems and fault-location methods) are introduced, and the NCS is developed and evaluated. In Section III, the FVMD + WVD method is described and simulated using PSCAD/EMTDC. In Sections IV and V, the experiments and conclusions are reported, respectively.

II. DESIGN AND CALIBRATION OF THE NCS

Double-terminal cable fault monitoring and location systems are composed of sensors, time synchronization modules, data-acquisition modules, and data-processing modules, with sensors being key components. Due to the abovementioned disadvantages of HFCT sensors, an NCS is developed in this study. This NCS is composed of a spherical-plate electrode, a signal circuit, a connecting bolt, and a shell, as depicted in Fig. 1.

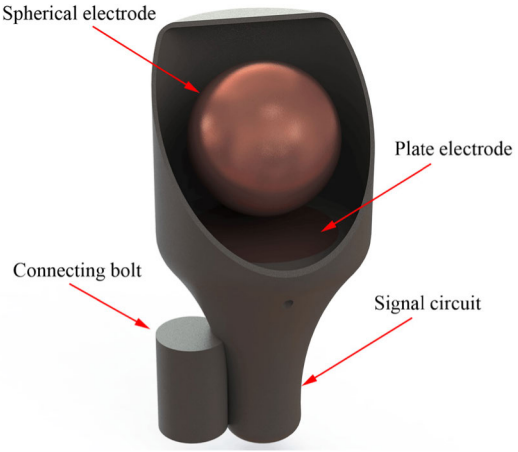

FIGURE 1. Components and structure of an NCS.

The NCS is a spherical plate capacitor, and thus the voltage between the spherical electrode and plate electrode varies with the electric field around the cable ends. Therefore, the data of traveling waves can be acquired by measuring the voltage of the NCS. During operation, the NCS is installed around the cable ends but not connected to the cable ends or the cable ground wires. Fig. 2 shows a double-terminal fault-detection and -location system that monitors a cable line that has a gas-insulated switchgear (GIS) and an outside end.

A schematic of a functional capacitor system containing an NCS is shown in Fig. 3 [27], where the parameters of this system are defined as follows:

C_{1g}: capacitance between the spherical electrode and the ground;

C_{2g}: capacitance between the plate electrode and the ground;

C_{tg}: capacitance between the cable end and the ground;

C_{12}: the capacitance of the spherical-plate capacitor;

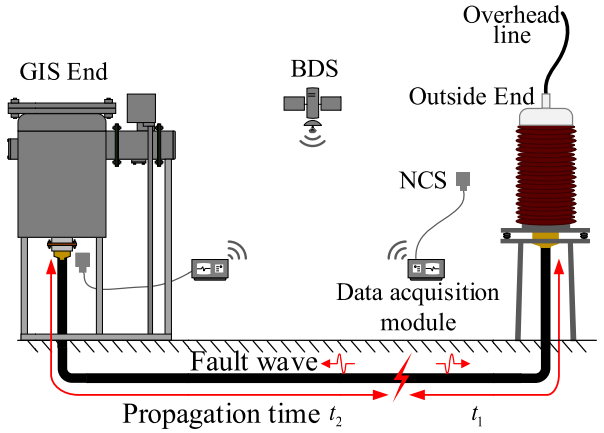

FIGURE 2. A double-terminal cable fault-detection and -location system.

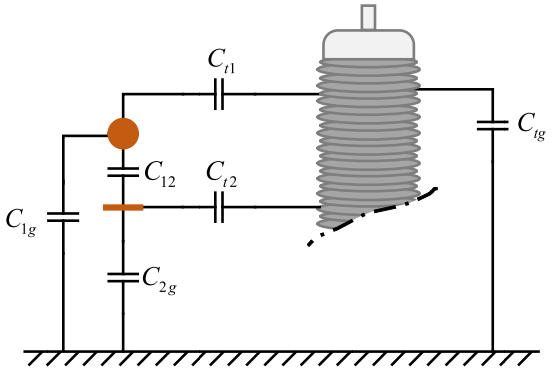

FIGURE 3. Schematic of a capacitor system comprising the NCS and a cable end.

C_{t1}: capacitance between the spherical electrode and the cable end;

C_{t2}: capacitance between the plate electrode and the cable end

Due to capacitor coupling, the NCS output voltage V_{12} can be derived from the cable fault voltage V_t, and the formulation is expressed as follows:

$$V_{12} = \frac{C_{t1}C_{2g} - C_{t2}C_{1g}}{(C_{t1} + C_{1g})(C_{t2}+C_{2g})+(C_{t1}+C_{t2}+C_{1g}+C_{2g})C_{12}} V_t \quad (1)$$

As described by (1), V_{12} can be adjusted by changing the values of the mutual capacitances. However, the mutual capacitances in Fig. 3 depend on the location of the NCS, and thus after the NCS has been installed, the only mutual capacitance that can be changed is C_{12}. Therefore, changing C_{12} is the only way to adjust the sensitivity of an NCS. Electromagnetic aspects [28] mean that C_{12} depends on many factors, such as the radius of the sphere and the circle plate (r_{sp}), the distance between the sphere and the plate (d_{sp}), and the dielectric parameter (ε) between the sphere and the plate. Nevertheless, changing d_{sp} is the most convenient and reliable approach in practice.

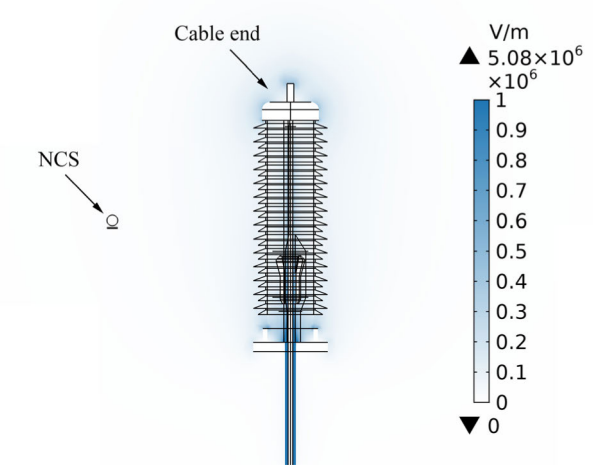

FIGURE 4. Simulation models and electric field simulation results.

The above mutual capacitors are irregular and finite geometric models. Thus, analytical methods, such as mirror methods and axis methods, cannot be used to calculate their mutual capacitances, whereas numerical methods, such as finite-element analysis methods, can be used. Thus, a model consisting of an NCS and cable end is established in COMSOL software to calculate the mutual capacitances. The materials and their relative permittivities are listed in Table 1 [29].

TABLE 1. Materials and their relative permittivity in simulation models.

Component	Material	Relative permittivity
Conductor	Copper	1×10^6
Stress cone	Silicone rubber	100
Shield of stress cone	Silicone rubber	2.8
Filler of insulation	Polyisobutylene	2.36
Insulator and busing	Silicone rubber	2.68
Top and bottom rings	Aluminum	1×10^6
Sensor	Copper	1×10^6
Enclosing domain	Air	1

The relationships between d_{sp}, r_{sp}, and the mutual capacitances are simulated and analyzed. For example, the distance from the NCS to the cable end is 1,000 mm, d_{sp} is 10 mm, r_{sp} is 35 mm, and the voltage of the cable end is 63.5 kV. The simulation models and electric-field simulation results are depicted in Fig. 4.

The mutual capacitances in Fig. 3 can be obtained via simulation, and are shown in Table 2.

TABLE 2. Mutual capacitances when d_{sp} = 10 mm and r_{sp} = 35 mm.

Mutual Capacitor	Capacitance(pF)
C_{t1}	0.515
C_{t2}	0.286
C_{1g}	0.298
C_{2g}	0.189
C_{tg}	411.534

C_{12} is simulated as d_{sp} changes from 2 mm to 20 mm and r_{sp} changes from 5 mm to 40 mm, and the curve is shown

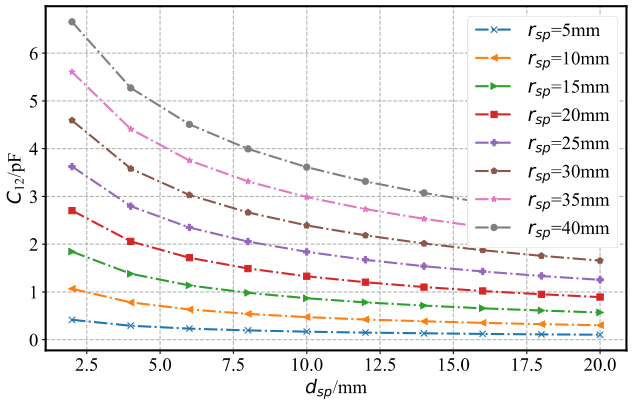

FIGURE 5. Curves of C_{12} vs d_{sp} for various values of r_{sp}.

in Fig. 5. After all of the mutual capacitances are obtained, they are substituted into (1), and thus the value of V_{12} is determined. Then, r_{sp} is varied depending on the value of V_{12}, and an adaptive NCS that suits the cable fault-location system is selected. The sensitivity of NCS can also be conveniently adjusted by changing the value of d_{sp}.

This section describes the development of the NCS and gives the derivation of the expression for V_{12}. In addition, the sensitivity adjustment curves of NCS are described by combining this expression for V_{12} with simulation information.

III. METHODS FOR THE IDENTIFICATION OF ARRIVAL TIMES

The method used for identifying the first wave-arrival times is the other key factor influencing the accuracy of cable fault location. In the following section, the FVMD + WVD method is proposed to identify the arrival time.

A. BASIC PRINCIPLE OF THE FVMD + WVD METHOD

FVMD is a signal processing approach that is based on Wiener filtering, the Hilbert transform, and frequency mixing. It can decompose a cable fault wave into a series of sparsity subsignals that have narrow bandwidths with different center frequencies. FVMD determines the optimal frequency and the narrowest bandwidth by iteration, whereas EMD does so by recursion. Thus, FWMD does not suffer from the aliasing phenomenon that is observed in EMD. FVMD comprises two parts: variational mode decomposition (VMD) and mode-order feedback. The constraint equation of optimal frequency and narrow bandwidth is as follows [30]:

$$\min_{\{u_k\},\{\omega_k\}} \left\{ \sum_k \left\| \partial_t \left[\left(\delta(t) + \frac{j}{\pi t} \right) * u_k(t) \right] e^{-j\omega_k t} \right\|_2^2 \right\}$$
$$\text{s.t.} \sum_k u_k = f(t) \tag{2}$$

where $\{u_k\} = \{u_1, u_2, \ldots, u_K\}$ and $\{\omega_k\} = \{\omega_k, \omega_2, \ldots, \omega_K\}$ are shorthand notation for the set of all modes and their center frequencies, respectively, and $f(t)$ is the original signal. Equation (2) is a constraint question, and a constraint can be reconstructed to solve it. Here, the quadratic penalty term α and Lagrangian multipliers $\lambda(t)$ are used to render the question unconstrained. Therefore, the augmented Lagrangian L is as follows:

$$\begin{aligned} &L(\{u_k\}, \{\omega_k\}, \lambda) \\ &= \alpha \sum_k \left\| \partial_t \left[\left(\delta(t) + \frac{j}{\pi t} \right) * u_k(t) \right] e^{-j\omega_k t} \right\|_2^2 \\ &\quad + \left\langle \lambda(t), f(t) - \sum_k u_k(t) \right\rangle \\ &\quad + \left\| f(t) - \sum_k u_k(t) \right\|_2^2 \end{aligned} \tag{3}$$

Equation (3) is denoted an original minimization problem or saddle-point problem, and it can be solved using the alternating direction method of multipliers (ADMM) [31]. The ADMM iteration equations of the mode $u_k(t)$ and the center frequency $\omega(t)$ are

$$\hat{u}_k(\omega) = \frac{\hat{f}(\omega) - \sum_{i \neq k} \hat{u}_i(\omega) + \frac{\hat{\lambda}(\omega)}{2}}{1 + 2\alpha(\omega - \omega_k)^2} \tag{4}$$

where $\hat{u}_k(\omega)$ is defined as the Wiener filtering of $u_k(t)$ and the mode in the time domain, $u_k(t)$ can be obtained from the real parts of the inverse Fourier transform, ω_k is the center of the corresponding mode's power spectrum. When $\hat{u}_k(\omega)$ meets the convergence condition (5) given below, $\hat{u}_k(\omega)$ and ω_k stop iterating.

$$\sum_k \frac{\left\| \hat{u}_k^{n+1} - \hat{u}_k^n \right\|_2^2}{\left\| \hat{u}_k^n \right\|_2^2} < \varepsilon \tag{5}$$

where $\hat{u}_k^{n+1}$ is n^{th} iteration of $u_k(t)$

In the above solution process, the mode order K must be preprovided, and it can influence the result of mode decomposition. To identify the mode order K, the feedback of the mode order is examined.

In the first step of the mode-order feedback process, the order k is initialized as 1, the wave signals are decomposed into two modes, and the similarity coefficients of the two modes are calculated by (6) [32]. Then, the modes are tested to determine whether they meet the convergence conditions given by (7). If they do not, the order $i = i + 1$, which has the largest similarity coefficient of the two modes, is subtracted from the wave signals. The residual wave signals are then decomposed into two new modes, which are re-tested using (7). These processes are repeated until the convergence conditions of (7) are satisfied, which means that the order K is $i + 1$. The formulation of the similarity coefficients δ_k^i of u_k^i is

$$\delta_k^i = \frac{\left| \sum_{t=1}^{N} u_k^i(t) f(t) \right|}{\sqrt{\sum_{t=1}^{N} \left(u_k^i(t) \right)^2 \sum_{t=1}^{N} (f(t))^2}} \tag{6}$$

where $u_k^i(t)$ represents the signal models with $k = 1$ or 2; and $f(t)$ represents the original fault-wave signals. The convergence conditions are as follows:

$$\max\left\{\delta_1^i, \delta_2^i\right\} < \min\left\{\delta_1^{i-1}, \delta_2^{i-1}\right\} \tag{7}$$

After FVMD, the fault waves of the cable are decomposed into several modes, ranging from low to high frequencies. The high-frequency components contain the fault-wave arrival time, which is generally a peak point. However, it is difficult to identify which peak point corresponds to the arrival time. However, given that the energies in equivalent capacitors and inductors are released gradually when a cable fault occurs, it follows that the time corresponding to the maximum energy is the fault-wave arrival time. Because the WVD has a higher resolution in the time and frequency domains than FVMD, it can be used to calculate nonstationary signals, such as the high-frequency components of a fault-wave energy distribution [33]. The WVD of cable fault-wave signals can be expressed as

$$W_f(t,\omega) = \int_{-\infty}^{\infty} f\left(t+\frac{\tau}{2}\right) f^*\left(t-\frac{\tau}{2}\right) \mathrm{e}^{-\mathrm{j}\omega t}\mathrm{d}\tau \tag{8}$$

where * denotes conjugation; and $f\left(t+\frac{\tau}{2}\right)f^*\left(t-\frac{\tau}{2}\right)$ is autocorrelation function of $f(t)$. The frequency ω in (8) is integrated from $-\infty$ to $+\infty$ to obtain the instantaneous energies of the fault-wave signal. The formula is as follows:

$$\begin{aligned} E_f(t) &= \int_{-\infty}^{\infty} W_f(t,\omega)\mathrm{d}\omega \\ &= \frac{1}{2\pi}\iint f\left(t+\frac{\tau}{2}\right)\cdot f^*\left(t-\frac{\tau}{2}\right)\mathrm{e}^{-\mathrm{j}\omega t}\mathrm{d}\tau\mathrm{d}\omega \\ &= \int f\left(t+\frac{\tau}{2}\right)\cdot f^*\left(t-\frac{\tau}{2}\right)\mathrm{d}\tau\cdot\frac{1}{2\pi}\int \mathrm{e}^{-\mathrm{j}\omega t}\mathrm{d}\omega \\ &= \int f\left(t+\frac{\tau}{2}\right)\cdot f^*\left(t-\frac{\tau}{2}\right)\delta(\tau)\,\mathrm{d}\tau = |f(t)|^2 \end{aligned} \tag{9}$$

In (9), the time corresponding to the maximum $E_f(t)$ is the fault-wave arrival time. Therefore, the fault location is given by

$$L_s = \frac{l + v\Delta t}{2} \tag{10}$$

where L_s is the distance from the start termination to the fault location; l is the length of the cable lines; v is the propagation velocity of the fault wave (which depends on the fault-wave frequency, which for cross-linked polyethylene cables is generally 1.72×10^8 m/s); and $\Delta t = t_s - t_e$ is the difference between the fault-wave arrival time at each end of the cable (where t_s is the fault-wave arrival time at the start of the cable and t_e is the fault-wave arrival time at the end of the cable).

The workflow of the FVMD + WVD method is depicted in the flowchart in Fig. 6.

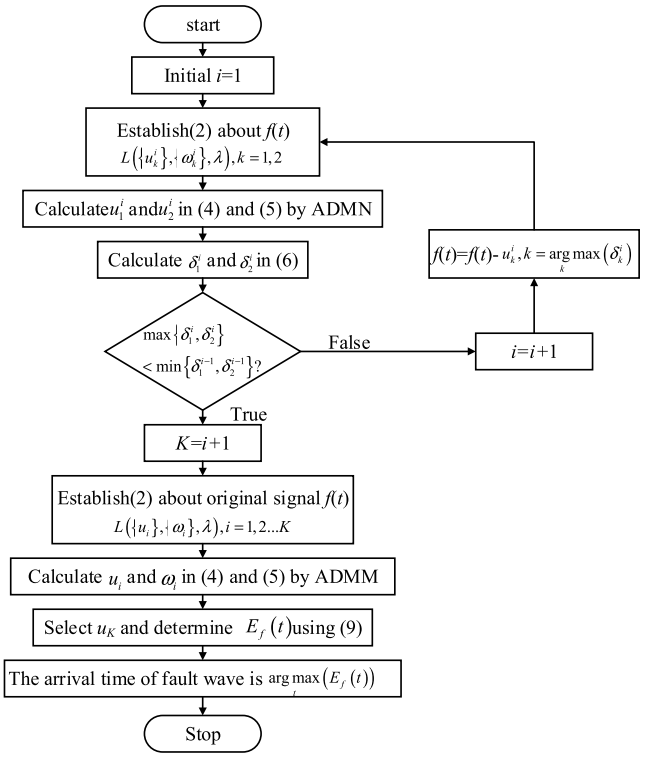

FIGURE 6. Workflow of the FVMD + WVD method.

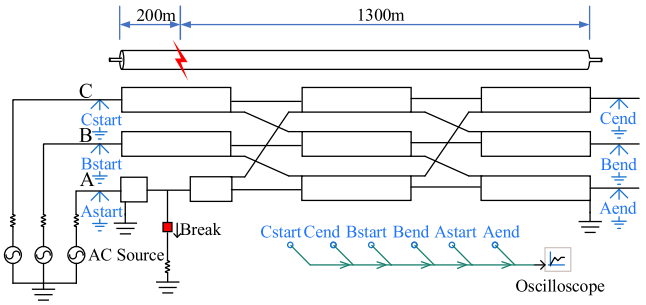

FIGURE 7. Simulation model of cable fault location.

B. SIMULATION AND VERIFICATION

In this section, the identification methods of the first wave arrival times are verified by simulation. In PSCAD/EMTDC, a 1.5-km-long 110-kV three-phase cable including a major cross-bonding section with a low-resistance fault is simulated. The low-resistance fault is located 0.5 km from the cable start. The simulation model is shown in Fig. 7.

The fault waves that arrive at the start and end terminations after the fault occurs, which are filtered by a high-pass filter, are depicted in Fig. 9. The modes of fault waves can be obtained by FVMD. For example, in Fig. 9, the fault wave of the head termination is decomposed into 10 modes, from low to high frequency, as depicted in Fig. 8.

The figure clearly shows that the peak value of the mode with the highest frequency corresponds to the arrival time of the fault wave. To further confirm the arrival time, the tenth intrinsic mode function (IMF10 mode) is solved using the WVD. The energy curve over time is depicted in Fig.9.

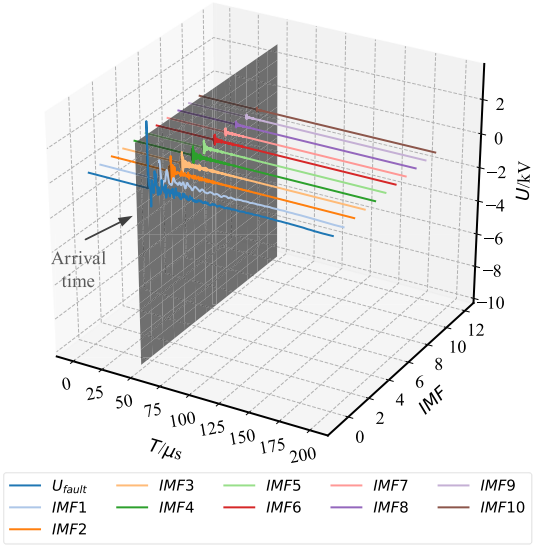

FIGURE 8. Mode decomposition results of the start termination fault wave obtained using FVMD.

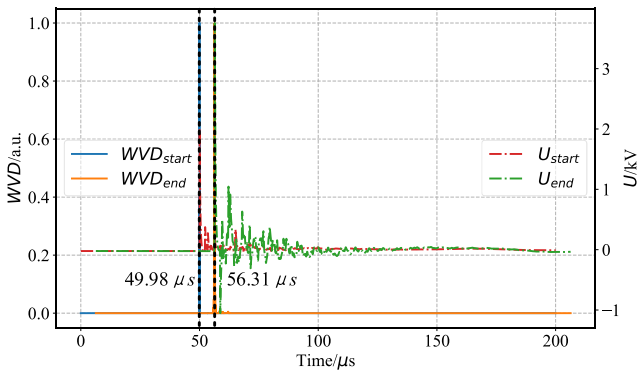

FIGURE 9. Energy distributions of the highest frequency modes.

The arrival times in Fig. 9 are then substituted into (10). The velocity of the fault wave calculated using the impedance and admittance matrices is 1.734×10^8 m/s, which reveals that fault is located 200 m from the start termination. As the default fault-location is 201.2 m, this result has an error of 0.08%. This error is largely due the dependence of the wave velocity on the fault-wave frequency; that is, because the fault wave includes components of various frequencies (from tens of kilohertz to several megahertz), its velocity is ambiguous.

In this section, an improved arrival-time identification method, the FVMD + WVD method, is developed, and the feasibility and accuracy of this new method are verified by simulation. This demonstrates that the location error is only 0.08%, which shows that method enables practical cable-fault location.

IV. EXPERIMENT AND VERIFICATION

To test the NCS and the FVMD + WVD fault-location method, a series of experiments are conducted. These comprise a DC experiment for NCS calibration and an AC experiment for cable location.

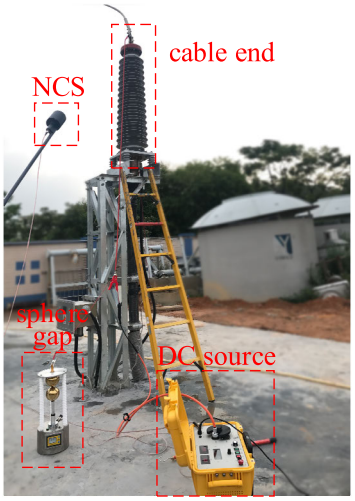

FIGURE 10. Setup of DC experiment for NCS calibration.

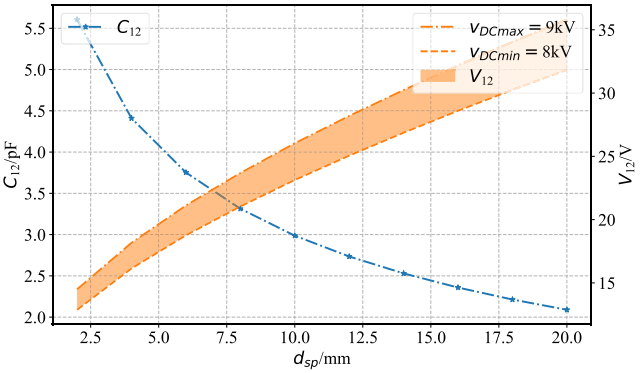

FIGURE 11. C_{12} vs d_{sp} curve for V_{12}.

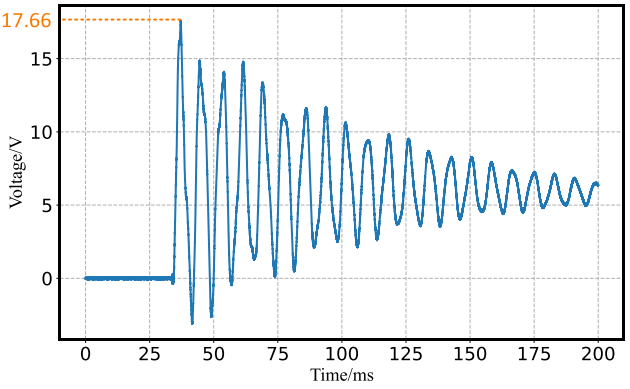

FIGURE 12. The fault wave measured by the NCS.

A. DC EXPERIMENT FOR NCS CALIBRATION

The setup of the DC experiment for calibration of the NCS system is composed of an adjustable DC source, a fault model simulated by a sphere gap, an NCS, and a 110-kV cable end. This setup is depicted in Fig. 10.

In this experiment, a DC source is applied to the cable end that is connected to the sphere gap. When this sphere gap is broken, a fault wave propagates through the wires to the cable end, and is detected by the NCS. The sphere gap is set to 2 mm and the breakdown voltage range measured by the DC

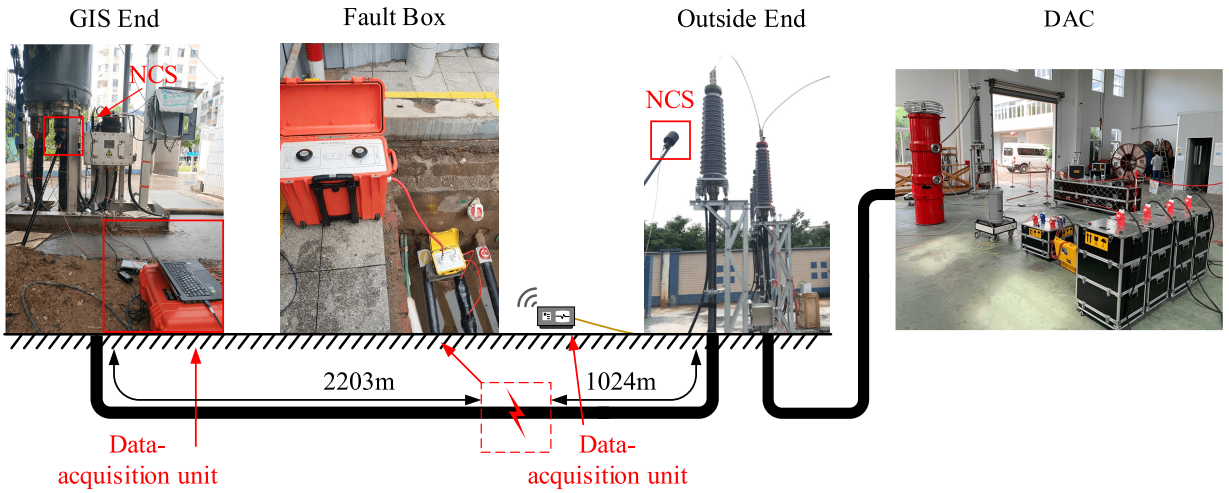

FIGURE 13. Setup of the cable fault-location experiment.

source is 8–9 kV. To obtain a suitable range of data, the NCS consists of a sphere and a plate with radii of 35 mm. Based on Fig. 5 and (1), the dependence of the NCS capacitance and voltage on d_{sp} can be obtained, as depicted in Fig. 11.

Data-acquisition limitations mean that the maximum voltage is 20 V. Based on the curve of V_{12} in Fig. 11, the NCS d_{sp} is adjusted to 5 mm. The breakdown voltage measured by the DC source is 8.2 kV, and the acquired data are shown in Fig. 12. The maximum measured voltage in Fig. 12 is 17.66 V. The theoretical value is 17.94 V (Fig. 10), which confirms that the NCS calibration curves in Fig. 5 provide an accurate reference for selecting and adjusting the NCS. Furthermore, the theoretical value is smaller than the measured value. This is due to the capacitances of the metal skeletons in the cable end being omitted to simplify calculations during the simulation, as these capacitances affect the mutual capacitors. In addition, the arc resistance affects the fault-wave voltage, which is smaller than the DC source-measurement voltage.

B. CABLE FAULT-LOCATION EXPERIMENT

The DAC technique has proven to be one of the most acceptable techniques for on-site partial discharge [34]. Therefore, a 110-kV DAC is used as the source in the cable fault-location experiment. The experiment is performed using an out-of-service 110-kV single-conductor power cable that is 3.227 km long. The experimental equipment are a DAC system, a fault box, NCSs, and data-acquisition devices that have a 1-Gs/s sampling frequency. The scheme of the experiment is shown in Fig. 13. The cable fault is controlled by the fault box and is a low-resistance fault located 1.024 km from the outside end of the cable. The fault waves at both ends are extracted with a bandpass filter. The fault waves and FVMD results are shown in Fig. 14.

Following the cable fault-location method proposed above, the high-frequency components of the fault-wave models, and the fault-wave decomposition results for the IMF11 at the GIS end and the IMF14 at the outside end, are analyzed using the

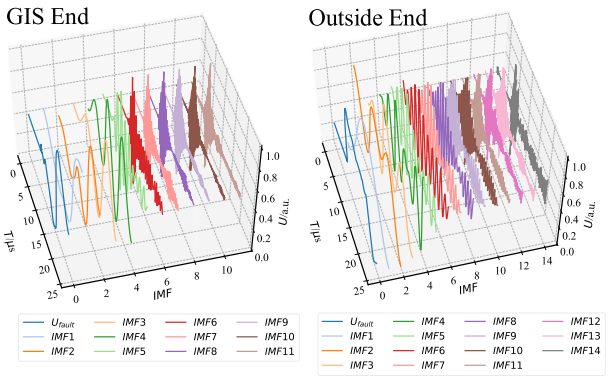

FIGURE 14. Fault waves and FVMD results at both cable ends.

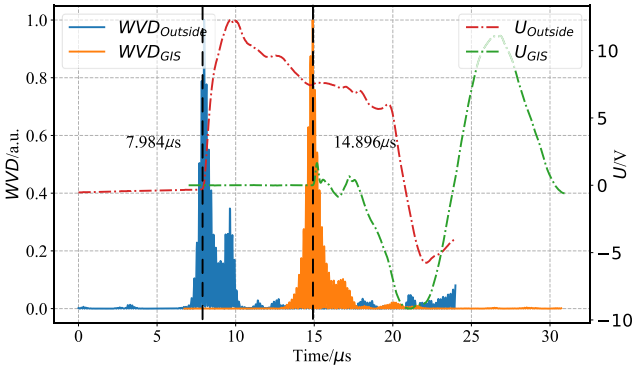

FIGURE 15. Energy distribution of the high-frequency components over time.

WVD. The energy distributions of the IMF11 and IMF14 are depicted in Fig. 15.

As shown in Fig. 15, the difference between the arrival times at the two ends is -6.912 μs, and the cable fault is located 1.0191 km from the outside end, as calculated by (10). Analysis of the result shows that the error is due to the inaccuracy of BDS/GPS synchronization and the influence of fault wave velocity. The average error of BDS/GPS synchronization is 20 ns, which is equivalent to 3.44 m of the fault-wave

TABLE 3. Comparison of results from different methods.

Method	Location of cable fault (km)	Relative error
Trigger level	1.0108	-1.29%
AIC	1.0122	-1.15%
Energy criterion	0.7549	-26.28%
Gabor	0.6861	-33.00%
FVMD + WVD	1.0191	-0.48%

The formulation of the relative error is $E_{re} = (L_c - L_p)/L_p$, where E_{re} is the relative error, L_c is the fault location calculated by various methods, and L_p is the actual fault location.

distance [35]. To test the accuracy of the FVMD + WVD method, the results from several fault-location methods [24] are compared in Table 3.

Table 3 shows that the FVMD + WVD method is more accurate than the other methods, and its relative error of −0.48% is acceptable for on-site cable fault location.

The results described in this section show that the calibration equations and charts of the NCS are suitably accurate for calibrating NCSs in DC experiments. In addition, a practical test of the FVMD + WVD method in an AC experiment using a 110-kV DAC system shows that it is more accurate than existing methods and enables significantly faster cable-fault location and power restoration.

V. CONCLUSION

In this study, an NCS is developed, and the output voltage of this novel sensor is analyzed theoretically. The sensitivity-adjustment curves of the NCS are described by theoretical calculations and simulations. Then, a novel fault-wave arrival-time identification method, the FVMD + WVM method, is developed, and its utility and accuracy are verified by simulation. Finally, a series of on-site experiments are performed, which reveal that the NCS effectively and accurately detects cable faults and that its sensitivity adjustment curves enable its sensitivity to be appropriately adjusted. In addition, the FVMD + WVD method is proven to be feasible and accurate, as it is more accurate in AC experiments than other current methods for the identification of fault-wave arrival time. Moreover, its location error of only −0.48% shows that is acceptable for practical cable-fault location. This work provides a novel adjustable sensor, a highly accurate cable fault-location method, and a new approach for cable fault detection and location.

REFERENCES

[1] (2019). *National Electric Power Reliability Annual Report*. National Energy Administration. 8th Congress, 1st Session. H. Con. Res. (Jun. 12, 2020). [Online]. Available: https://prpq.nea.gov.cn/ndbg

[2] A. J. Reid, C. Zhou, D. M. Hepburn, M. D. Judd, W. H. Siew, and P. Withers, "Fault location and diagnosis in a medium voltage EPR power cable," *IEEE Trans. Dielectr. Electr. Insul.*, vol. 20, no. 1, pp. 10–18, Feb. 2013.

[3] Z. Chuanzong, L. Chuanbo, W. Qinghao, Z. Wenguang, J. Hongzhi, G. Changxin, and S. Yang, "The role of DC voltage endurance test in the cable fault nature determination," in *Proc. IEEE PES Innov. Smart Grid Technol.*, Tianjin, China, May 2012, pp. 1–3.

[4] J. Zhang, Y. Zhang, and Y. Guan, "Analysis of time-domain reflectometry combined with wavelet transform for fault detection in aircraft shielded cables," *IEEE Sensors J.*, vol. 16, no. 11, pp. 4579–4586, Jun. 2016.

[5] T. C. Henneberger and P. G. Edwards, "Bridge methods for locating resistance faults on cable wires," *Bell Syst. Tech. J.*, vol. 10, no. 3, pp. 382–407, Jul. 1931.

[6] A. A. Girgis, C. M. Fallon, and D. L. Lubkeman, "A fault location technique for rural distribution feeders," *IEEE Trans. Ind. Appl.*, vol. 29, no. 6, pp. 1170–1175, Nov. 1993.

[7] R. Dashti, S. M. Salehizadeh, H. R. Shaker, and M. Tahavori, "Fault location in double circuit medium power distribution networks using an impedance-based method," *Appl. Sci.*, vol. 8, no. 7, pp. 1–15, Jul. 2018.

[8] F. H. Magnago and A. Abur, "Fault location using wavelets," *IEEE Trans. Power Del.*, vol. 13, no. 4, pp. 1475–1480, Oct. 1998.

[9] M. M. Saha, J. J. Izykowski, and E. Rosolowski, "Fault location-basic concept and characteristic of methods," in *Fault Locaiton on Power Networks*, 1st ed. Berlin, Germany: Springer, 2010, ch. 1, sec. 5, pp. 9–25.

[10] R. Salim, K. Salim, and A. Bretas, "Further improvements on impedance-based fault location for power distribution systems," *IET Gener. Transmiss. Distrib.*, vol. 5, no. 4, pp. 467–478, Apr. 2011.

[11] R. Krishnathevar and E. E. Ngu, "Generalized impedance-based fault location for distribution systems," *IEEE Trans. Power Del.*, vol. 27, no. 1, pp. 449–451, Jan. 2012.

[12] L. Wang, H. Liu, L. V. Dai, and Y. W. Liu, "Novel method for identifying fault location of mixed lines," *Energies*, vol. 11, no. 6, pp. 1–19, Jun. 2018.

[13] Y. Chen, D. Liu, and B. Xu, "Wide-area traveling wave fault location system based on IEC61850," *IEEE Trans. Smart Grid*, vol. 4, no. 2, pp. 1207–1215, Jun. 2013.

[14] R. Liang, G. Fu, X. Zhu, and X. Xue, "Fault location based on single terminal travelling wave analysis in radial distribution network," *Int. J. Electr. Power Energy Syst.*, vol. 66, pp. 160–165, Mar. 2015.

[15] S. Lan, M.-J. Chen, and D.-Y. Chen, "A novel HVDC double-terminal non-synchronous fault location method based on convolutional neural network," *IEEE Trans. Power Del.*, vol. 34, no. 3, pp. 848–857, Jun. 2019.

[16] F. M. Aboshady, M. Sumner, and D. W. P. Thomas, "A double end fault location technique for distribution systems based on fault-generated transients," in *Proc. IEEE 26th Int. Symp. Ind. Electron. (ISIE)*, Edinburgh, U.K., Jun. 2017, pp. 32–36.

[17] J. Liang, T. Jing, H. Niu, and J. Wang, "Two-terminal fault location method of distribution network based on adaptive convolution neural network," *IEEE Access*, vol. 8, pp. 54035–54043, Mar. 2020.

[18] Q. Zhang, J. Zhu, J. Jia, F. Tao, and L. Yang, "Design of a current transducer with a magnetic core for use in measurements of nanosecond current pulses," *Meas. Sci. Technol.*, vol. 17, no. 4, pp. 895–900, Mar. 2006.

[19] W. He, H. Li, D. Liang, H. Sun, C. Yang, J. Wei, and Z. Yuan, "Implementation of a novel double-side technique for partial discharge detection and location in covered conductor overhead distribution networks," *Meas. Sci. Technol.*, vol. 26, no. 12, Nov. 2015, Art. no. 125009.

[20] F. Xu, X. Wang, and H. Wu, "Inspection method of cable-stayed bridge using magnetic flux leakage detection: Principle, sensor design, and signal processing," *J. Mech. Sci. Technol.*, vol. 26, no. 3, pp. 661–669, Mar. 2012.

[21] W. X. Pan, K. Zhao, C. Xie, X. R. Li, J. Chen, and L. B. Hu, "Distributed online monitoring method and application of cable partial discharge based on φ-OTDR," *IEEE Access*, vol. 7, pp. 144444–144450, Sep. 2019.

[22] A. Marinescu, I. Dumbrava, and L. Mandache, "PD measurement at large capacitors using a modified HFCT," in *Proc. IEEE Int. Conf. High Voltage Eng. Appl. (ICHVE)*, Athens, Greece, Sep. 2018, Art. no. 18469252.

[23] C. Herold, T. Leibfried, S. Markalous, and I. Quint, "Algorithms for automated arrival time estimation of partial discharge signals in power cables," in *Proc. Int. Symp. High Volt. Eng. (ISH)*, Budapest, Hungary, 2019, p. 332.

[24] P. Wagenaars, P. A. A. F. Wouters, P. C. J. M. Van Der Wielen, and E. F. Steennis, "Accurate estimation of the time-of-arrival of partial discharge pulses in cable systems in service," *IEEE Trans. Dielectr. Electr. Insul.*, vol. 15, no. 4, pp. 1190–1199, Aug. 2008.

[25] R. Mardiana and C. Q. Su, "Phase difference method for two-end partial discharge location in power cables," in *Proc. IEEE GCC Conf. Exhib. (GCC)*, Dubai, United Arab Emirates, Feb. 2011, pp. 597–600.

[26] R. J. Hamidi and H. Livani, "A recursive method for traveling-wave arrival-time detection in power systems," *IEEE Trans. Power Del.*, vol. 34, no. 2, pp. 710–719, Apr. 2019.

[27] W. Zhang, Z. Hou, H.-J. Li, C. Liu, and N. Ma, "An improved technique for online PD detection on covered conductor lines," *IEEE Trans. Power Del.*, vol. 29, no. 2, pp. 972–973, Apr. 2014.

[28] B. S. Guru and H. R. Hiziroglu, "Electrostatics," in *Electromagnetic Field Theory Fundamentals*, 2nd ed. Camridge, U.K.: CUP, 2004, ch. 3, sec. 10, pp. 70–129.

[29] C. Zachariades, V. Peesapati, T. Gardner, and O. Cwikowski, "Electric field and thermal analysis of 132 kV ceramic oil-filled cable sealing ends," *IEEE Trans. Power Del.*, vol. 29, no. 2, pp. 972–973, Jan. 2014.
[30] K. Dragomiretskiy and D. Zosso, "Variational mode decomposition," *IEEE Trans. Signal Process.*, vol. 62, no. 3, pp. 531–544, Feb. 2014.
[31] M. R. Hestenes, "Multiplier and gradient methods," *J. Optim. Theory Appl.*, vol. 4, no. 5, pp. 303–320, Nov. 1969.
[32] Z. J. Zhao, Y. B. Huang, F. F. Qiang, and A. F. Yang, "Single channel blind source separation algorithm based on feedback variational mode decomposition," *J. Vib. Shock*, vol. 38, no. 13, pp. 268–273, Jul. 2019.
[33] G. Chen, J. Chen, and G. M. Dong, "Chirplet Wigner–Ville distribution for time–frequency representation and its application," *Mech. Syst. Signal Process.*, vol. 41, nos. 1–2, pp. 1–13, Dec. 2013.
[34] Y. Lu, X. Zhao, Y. Geng, H. Li, X. Xu, W. He, S. Yang, and Y. Yan, "A low-cost DAC system for on-site PD testing of HV cables based on ACRF and capacitor bank," *IEEE Trans. Power Del.*, vol. 35, no. 5, pp. 2551–2553, Oct. 2020.
[35] F. Mohamed, W. Siew, J. Soraghan, S. Strachan, and J. McWilliam, "Partial discharge location in power cables using a double ended method based on time triggering with GPS," *IEEE Trans. Dielectr. Electr. Insul.*, vol. 20, no. 6, pp. 2212–2221, Dec. 2013.

MING ZHANG received the B.S. and M.S. degrees from Wuhan University, Wuhan, China, in 1997 and 2010, respectively.

He works in Foshan Electric Power Station of Guangdong Power Grid Company Ltd. He is the author of more than 20 articles. His research interests include the emergency repair of transmission lines and rapid power supply transferring technology. He was a recipient of 15 awards about Science and Technology Progress Award from Guangdong Power Grid Company Ltd.

KUN ZHAO (Student Member, IEEE) received the B.S. degree in electrical engineering from the China University of Mining and Technology, Xuzhou, China, in 2017, and the M.S. degree in high voltage and insulation technology from Hohai University, Nanjing, China, in 2020. He is currently pursuing the Ph.D. degree in electrical engineering with Xi'an Jiaotong University, Xi'an, China.

His main research interest includes high voltage and insulation technology.

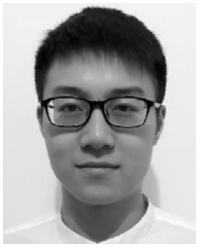

YUAN YAN received the B.S. degree in electrical engineering from Xi'an Jiaotong University, Xi'an, China, in 2016, where he is currently pursuing the Ph.D. degree in electrical engineering.

His main research interest includes high voltage and insulation technology.

YUXIN LU received the B.S. degree in electrical engineering from Xi'an Jiaotong University, Xi'an, China, in 2017, where he is currently pursuing the Ph.D. degree.

His main research interest includes high voltage and insulation technology.

SAIKE YANG received the B.S. degree in electrical engineering from North China Electric Power University, Baoding, China, in 2017. He is currently pursuing the Ph.D. degree in electrical engineering with Xi'an Jiaotong University, Xi'an, China. His research interests include insulation condition monitoring of the electrical equipment, modeling, and numerical analysis of electromagnetic.

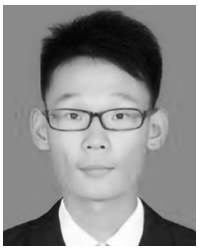

LI WANG received the B.S. degree in electrical engineering from North China Electric Power University, Baoding, China, in 2019. He is currently pursuing the Ph.D. degree in electrical engineering with Xi'an Jiaotong University, Xi'an, China.

His research interest includes partial discharge detection on medium voltage cables.

HONGJIE LI received the B.S., M.S., and Ph.D. degrees from Xi'an Jiaotong University, Xi'an, China, in 1989, 1992, and 1998, respectively.

In 1997, he was a Visiting Scholar with Osaka University, Osaka, Japan. From 1999 to 2001, he was a Research Fellow on insulation condition monitoring with Nanyang Technological University, Singapore. From 2001 to 2007, he was with Singapore's National Grid Company Ltd. He is currently a Professor with the High Voltage Division, School of Electrical Engineering, Xi' an Jiaotong University. His major research interests include insulation condition monitoring of the electrical equipment, modeling, and numerical analysis of electromagnetic devices.